

# **Kanamycin uptake into *Escherichia coli* is facilitated by OmpF and OmpC porin channels located in the outer membrane**

*Jayesh Arun Bafna*,<sup>1‡</sup> *Eulàlia Sans-Serramitjana*,<sup>1‡</sup> *Silvia Acosta-Gutiérrez*,<sup>2‡</sup> *Igor Bodrenko*<sup>3</sup>,  
*Daniel Hörömpöli*,<sup>4,5</sup> *Anne Berscheid*,<sup>4,5</sup> *Heike Brötz-Oesterhelt*,<sup>4,5,\*</sup> *Mathias Winterhalter*<sup>1,\*</sup> and  
*Matteo Ceccarelli*<sup>3,6,\*</sup>.

<sup>1</sup> Department of Life Sciences and Chemistry, Jacobs University Bremen, D-28719 Bremen, Germany

<sup>2</sup> Department of Chemistry, University College London, WC1E 6BT London, United Kingdom

<sup>3</sup> IOM/CNR, Sezione di Cagliari, Cittadella Universitaria di Monserrato, 09042 Monserrato, Italy.

<sup>4</sup> Department of Microbial Bioactive Compounds, Interfaculty Institute of Microbiology and Infection Medicine, University of Tübingen, D-72076 Tübingen, Germany

<sup>5</sup> German Center for Infection Research (DZIF), partner site D-72076 Tübingen, Germany

<sup>6</sup> Department of Physics, University of Cagliari, and CNR/IOM, Cittadella Universitaria di Monserrato, 09042 Monserrato, Italy.

‡ Equally contributed

Despite decades of therapeutic application of aminoglycosides, it is still a matter of debate if porins contribute to the translocation of the antibiotics across the bacterial outer membrane. Here, we quantified the uptake of kanamycin across the major porin channels OmpF and OmpC present in the outer membrane of *Escherichia coli*. Our analysis revealed that, despite its relatively large size, about 10 - 20 kanamycin molecules per second permeate through OmpF and OmpC under a 10  $\mu$ M concentration gradient, whereas OmpN does not allow the passage. Molecular simulations elucidate the uptake mechanism of kanamycin through these porins. Whole-cell studies with a defined set of *E. coli* porin mutants provide evidence that translocation of kanamycin *via* porins is relevant for antibiotic potency. The values are discussed with respect to other antibiotics.

**KEYWORDS** *E. coli*, OmpF, OmpC, OmpN, bacterial porins, optimal transport

The complex cell envelope of Gram-negative bacteria comprises two membranes: the outer membrane (OM) and the cytoplasmic membrane. The two membranes delimit the periplasmic space of the bacterial cell and prevent the accumulation of toxic agents in the cytosol while regulating the access of nutrients vital for growth and cell function. The OM is the first barrier during compound uptake. It is composed of an asymmetric bilayer: an inner leaflet of phospholipids and an outer leaflet of lipopolysaccharides (LPS). Both OM leaflets combined prevent the efficient diffusion of hydrophilic as well as hydrophobic molecules. Porins, water-filled channels spanning across the OM, enable passive diffusion of small, hydrophilic molecules into the periplasm. Substrate specificity is mainly defined by the constriction zone within the barrel structure of these porins, determining entry of molecules by factors such as size, shape, electric multipoles, and rigidity.<sup>1,2,3</sup>

*E. coli* encodes multiple porins. The major porins OmpF and OmpC are highly abundant and both cation-selective, and it has been thought that they restrict the passage to compounds with a size-exclusion limit of about 600 Da.<sup>4</sup> However, it has recently been suggested that this limit should be redefined using other parameters.<sup>5,6</sup> The translocation of several classes of antibiotics, e.g.  $\beta$ -lactams and fluoroquinolones, through porins has been investigated extensively. Also, porin modification emerged as antibiotic resistance mechanism in clinical isolates,<sup>7</sup> based on specific changes in amino acid residues or decreased expression of wild-type porins.<sup>8</sup>

Aminoglycosides (AGs) target the ribosome in the cytoplasm, thus they have to overcome both membranes in Gram-negative bacteria. Despite their frequent use as therapeutic agents, the mechanisms of their OM translocation remain incompletely understood. The self-promoted pathway is a proposed uptake mechanism. Here, divalent cations between LPS molecules are displaced by AGs, which leads to brief OM destabilization, thereby enabling OM translocation.<sup>9</sup>

However, since AGs are both cationic and hydrophilic structures with a molecular size below 600 Da, they have also been hypothesized to diffuse through porins of *E. coli*. First *in vitro* assays using the liposome swelling technique had suggested translocation of various aminoglycosides through *E. coli* porins,<sup>10</sup> but whole-cell experiments were inconclusive and contradictory.<sup>9,11</sup>

To elucidate the passage of AGs through *E. coli* porins, we characterized the permeability of kanamycin through three outer membrane porins of *E. coli*, namely OmpF, OmpC and the structurally similar OmpN. We quantified the uptake by an electrophysiological zero-current assay using concentration gradients of kanamycin under bi-ionic conditions, and combined it with single-channel measurements to determine the net flux of kanamycin.<sup>12,13</sup> Our single-channel study in the presence of low amounts of kanamycin revealed clear blockages. Thus, we analysed also the change in event rates with increasing transmembrane applied voltage. To reveal the main interactions of kanamycin while diffusing along the pore, we examined the translocation event of kanamycin through OmpF and OmpC employing enhanced sampling molecular dynamics simulations. We could confirm these new insights in whole-cell assays, where the double deletion of both porin genes *ompF* and *ompC* decreased kanamycin susceptibility. A single deletion of only one of these porins had no detectable effect on kanamycin resistance, which corroborates that both major porins OmpF and OmpC play a role in kanamycin translocation across the OM of *E. coli*. Combining the electrophysiological data, all-atom simulations and whole-cell results, we conclude that both OmpF and OmpC are permeable to kanamycin.

## RESULTS

### Experimental flux quantification using reversal potential measurements:

We have previously shown that the net flux of charged compounds driven by a concentration gradient can be estimated from the experimentally accessible reversal potential, in combination with single channel conductance recordings.<sup>12</sup> In a first series of experiments, the three porins of interest from the *E. coli* outer membrane (OmpF, OmpC and OmpN) were reconstituted into a planar bilayer, and the single channel currents in the presence of kanamycin sulphate, and potassium sulphate as control, were recorded. **Table S1** summarizes the conductance measurements of the three *E. coli* porins obtained in symmetrical 20 mM kanamycin sulphate or K<sub>2</sub>SO<sub>4</sub> at pH 7 and  $\Delta V=+100$  mV. Due to the diverse size of the cations (kanamycin *versus* K<sup>+</sup>, see Table S3 for a comparison with pore sizes), the single trimeric channel conductance with K<sub>2</sub>SO<sub>4</sub> was substantially higher than that with kanamycin sulphate: 240 pS *vs.* 16 pS, respectively, for OmpF. Moreover, OmpF conductance was comparable to that of OmpC, whereas OmpN conductance was significantly lower (16:13:9.5 pS in case of kanamycin sulphate or 240:180:58 pS in case of KCl).

To further quantify the concentration-driven flux, we applied a concentration gradient and recorded the induced voltage to obtain the permeability ratio. The latter was obtained by fitting the experimental I-V curves to the Goldman-Hodgkin-Katz (GHK) current equation.<sup>14</sup> Despite the fact that the assumptions of the GHK-theory (point-like non-interacting ions in a homogeneous electric field) are not fulfilled, we expect in general a reasonably good prediction for the ion permeability ratio.<sup>12</sup> We used a bi-ionic symmetrical 20 mM of kanamycin and 35 mM of the sulphate salt on both sides of the membrane containing, respectively, OmpF, OmpC or OmpN porins (the difference in the concentrations is due to the titration of H<sub>2</sub>SO<sub>4</sub> for adjusting the pH to 7). The *cis* compartment was then supplemented with 50 mM of kanamycin

and 87.5 mM of the sulphate salt and the zero-current-potential was measured (**Fig. S1 A-C**). As summarized in **Table 1**, the reversal potentials, in the case of kanamycin sulphate, are negative for the same ionic concentrations *cis/trans* for the three porins assessed, with the maximal reversal potential value for the OmpN porin. This implies that anions permeate faster compared to cations in all three channels, with OmpN almost impermeable to kanamycin. In contrast, the reversal potentials in the case of potassium sulphate are positive for the same ionic concentration gradients *cis/trans* for the three porins studied, with the highest cation selectivity for OmpN. Our results are in agreement with the qualitative observation of the permeation specificities by Nikaido and Prilipov *et al.*<sup>15,16</sup>

**Table 1.** Reversal potential permeability measurements. Determined zero current potentials ( $V_{rev}$ ) with standard deviation, calculated permeability ratios and flux-rate from the mean zero current potential. \* Permeability ratio is too small to estimate the flux.

Channel	(trans-side) (mM)		(GND/cis-side) (mM)		$V_{rev}$ (mV)	P = $P_{Kan^{4+}}/$ $P_{sulphate^{2-}}$	Flux extrapolated to 10 $\mu$ M ion gradient (molecules/s)	
	Kanamycin	SO <sub>4</sub> <sup>2-</sup>	Kanamycin	SO <sub>4</sub> <sup>2-</sup>			Cations	SO <sub>4</sub> <sup>2-</sup>
OmpF	20	35	50	87.5	-8.7 ± 2.5	1:14	9	73
OmpC	20	35	50	87.5	-5.1 ± 0.6	1:4.2	16	20
OmpN	20	35	50	88.4	-12.0 ± 3	1:>600 *	too low	
	K <sup>+</sup>	SO <sub>4</sub> <sup>2-</sup>	K <sup>+</sup>	SO <sub>4</sub> <sup>2-</sup>		$P_{K^+}/P_{sulphate^{2-}}$		
OmpF	100	50	500	250	10.7 ± 0.7	2.4:1	1,300	1,100
OmpC	100	50	500	250	13.4 ± 1.2	2.8:1	800	600
OmpN	20	10	100	50	33.5 ± 3.1	21:1	900	100

In a second series of measurements, we recorded the permeation of single kanamycin with single channel electrophysiology. Reconstituted OmpF, OmpC or OmpN showed a stable conductance in their open conformation. In the membrane potential range used in these experiments, from  $-150\text{ mV}$  to  $+150\text{ mV}$ , the channel open conductance is ohmic, with  $\approx 4\text{ nS}$  for OmpF,  $\approx 2.7\text{ nS}$  for OmpC and  $\approx 1.6\text{ nS}$  for OmpN, all at  $1\text{ M KCl}$ . Throughout this study, the membrane potential was defined as positive on the *trans*-side of the chamber, the *cis*-side being the virtual ground, and the respective channel was inserted into the bilayer from the *cis*-side of the chamber, unless otherwise noted.

After successful single channel reconstitution was achieved, the ion current was recorded for 30 s at each applied potential from ( $+150\text{ mV}$  to  $-150\text{ mV}$ ), then  $10\text{ }\mu\text{M}$  of kanamycin sulphate was added to the *cis*-side of the chamber and their translocation was investigated under the applied membrane potential (note the solution was buffered with  $10\text{ mM HEPES}$ , the pH was stable at pH 7). The entry of kanamycin molecules into the constriction zone of the porin causes a resolvable reduction in the open pore conductance with resolvable dwell times ( $\tau_d > 0.1\text{ ms}$ ), referred to as “events” in this work. Figure 1A-C shows the current traces of the porins in the presence of  $10\text{ }\mu\text{M}$  of kanamycin sulphate with resolvable events at a membrane potential of  $-100\text{ mV}$ . We analyzed the event rates  $f_e$  and mean dwell times  $\tau_d$ , to assess the translocation of these molecules through these general diffusion porins, where  $\tau_d$  is obtained from fitting an exponential to the distribution of dwell times and  $N_e$  is the number of events in a given time interval. For calculation of  $\tau_d, f_e$  at least  $\sim 1000$  events were analysed.

The results of the analysis of  $\tau_d$  and  $f_e$  are shown in Figure 2 for OmpF, OmpC, and OmpN. The event rate increases throughout. However, an event rate itself does not allow drawing conclusions on the translocation.<sup>17</sup> The decrease of the dwell time at high voltage is a signature

of translocation. In the case of OmpF, Figure 2B (black filled squares) shows the maximum of dwell time at around -75 mV. This may indicate that kanamycin ions translocate with higher probability through OmpF above this potential, although a significant increase in  $f_e$  is observed (Figure 2A, filled black square).<sup>18</sup> In case of OmpC, we see a clear trend in the dwell time pattern (decreasing dwell time with increasing transmembrane potential), which again may hint towards the enhanced translocation of kanamycin through OmpC. From the permeability ratios obtained by reversal potential measurements of OmpF and OmpC, we see that kanamycin should permeate better through OmpC than OmpF at low concentrations (Table 1). However, the entry rate  $f_e$  in OmpF shows saturation at high voltages, which is not observed for OmpC. When extrapolating the flux obtained at high concentrations (reversal potential) to low concentrations (single channel), one needs to account for the saturation of OmpF. Indeed, we expect both values to be rather similar at low kanamycin concentrations. While OmpN shows an increasing number of event rates (Figure 2A, blue filled triangles) at high voltages, their respective dwell times shown in Figure 2B, (blue filled triangle) are voltage independent, which means rather caused by short-lived (bounce back) events.<sup>18</sup>

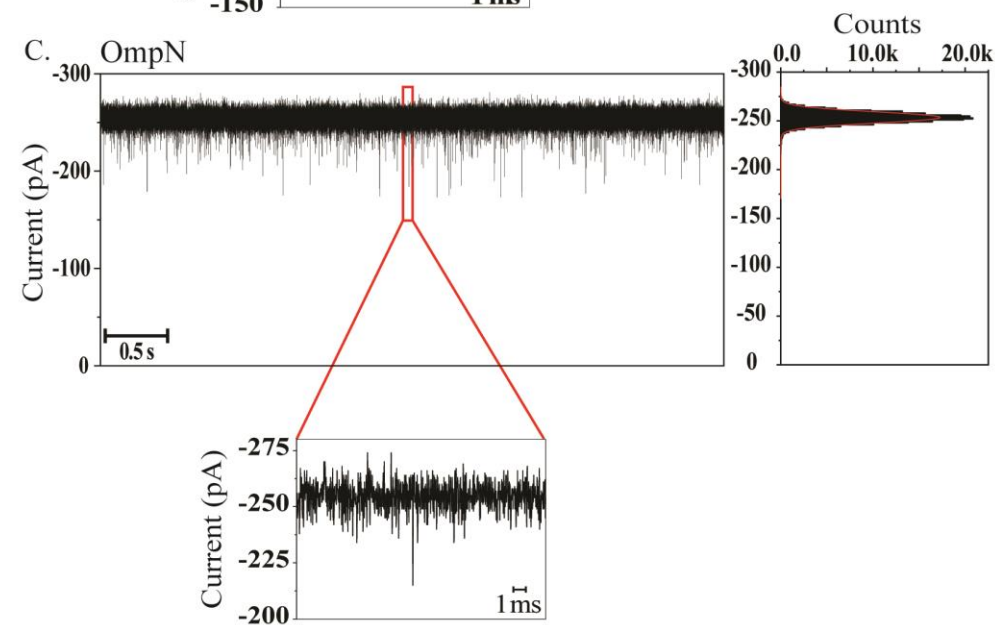
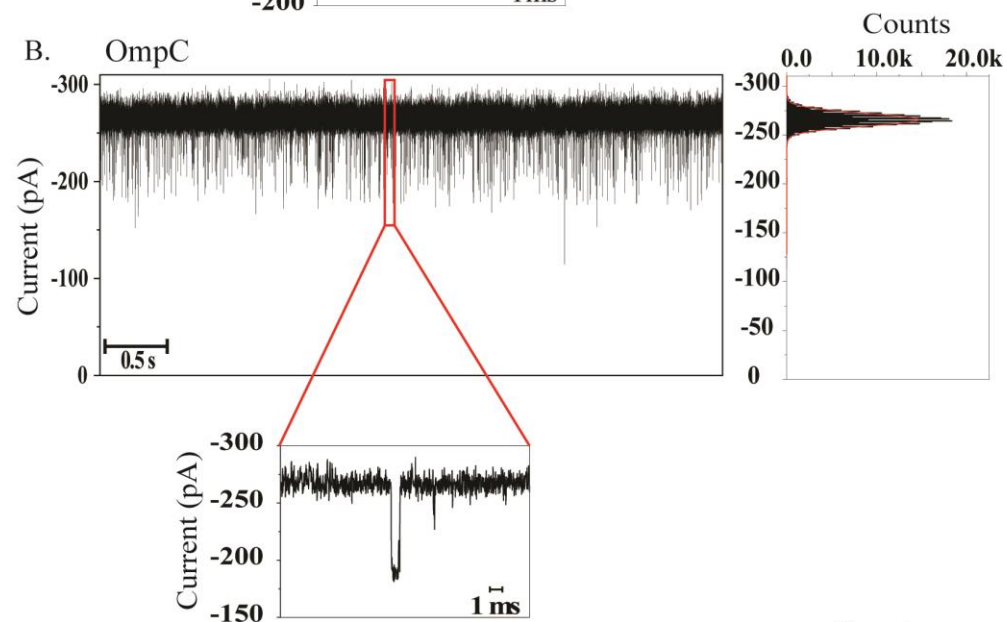
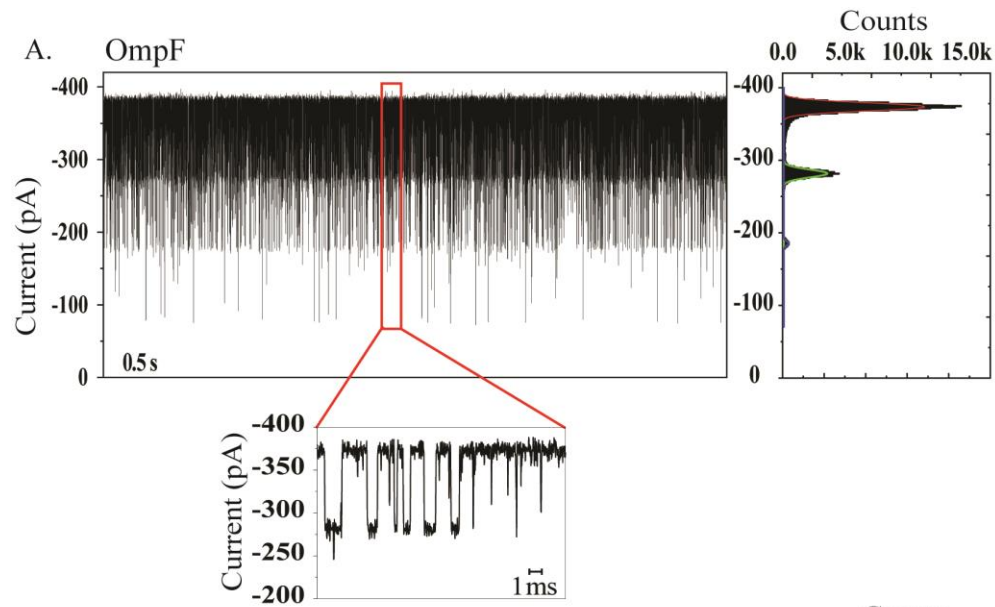


**Figure 1. Ion current traces in the presence of kanamycin.** Single channel measurements of A) OmpF, B) OmpC and C) OmpN in the presence of 10  $\mu$ M kanamycin sulphate in 1M KCl, 10 mM HEPES at pH 7. Figure 1A is the single channel trace of OmpF in the presence of kanamycin sulphate at an applied potential of -100 mV. Its corresponding zoom of the events and all point histogram are on the right. Similarly, Figure 1B and 1C show, respectively, the traces of OmpC and OmpN, with their zoomed events and all point histograms.

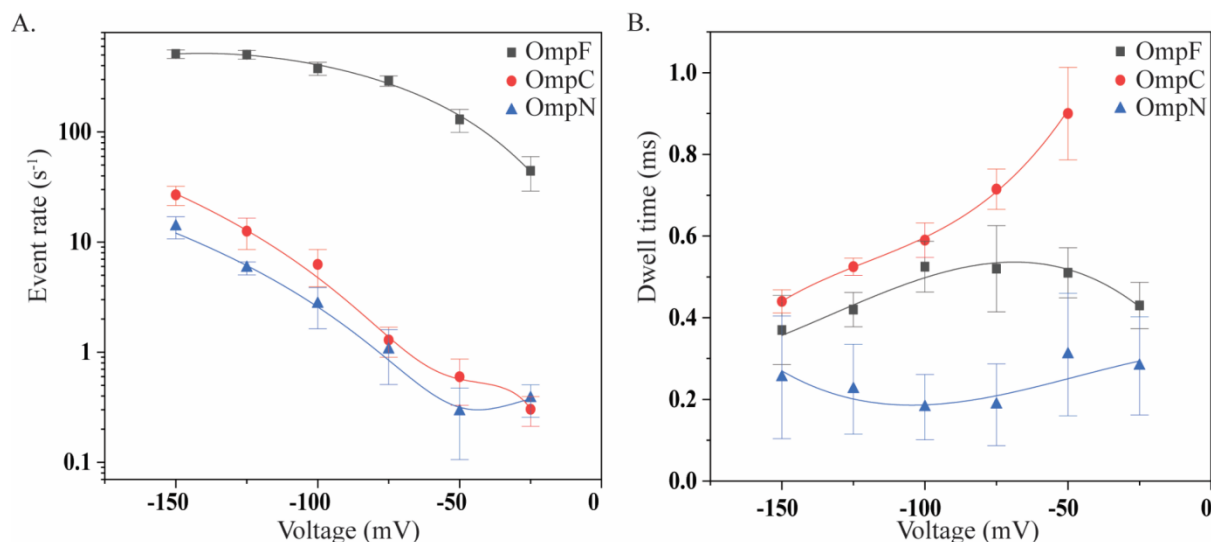


**Figure 2. Event rates and dwell times.** Statistical analysis of the traces measured at different applied voltages for OmpF, OmpC and OmpN of figure 1. A) Event rate  $f_e$  vs applied negative voltages. Increasing the negative voltage pulls more cationic kanamycin molecules into the channel. B) Dwell time analysis. In the case of OmpC, higher negative voltage drives kanamycin faster through the channel, whereas in OmpF only voltages above -75 mV reduce the residence time. Note that at low voltages up to -75 mV kanamycin is less prone to permeate and is rather pushed against the inner barrier. In contrast for OmpN, the dwell time is independent of the voltage indicating mainly non-translocating events. The black, red and blue lines are intended to serve as guidelines for the reader to follow the data points.

### Translocation mechanism through the main porins of *E. coli* (molecular dynamics)

Starting from the available high-resolution structures of OmpF and OmpC, we used enhanced sampling molecular dynamics simulations (metadynamics) to provide an atomistic view of the main interactions of kanamycin within the channel, when translocating from CIS to TRANS. In previous works,<sup>6,19–21</sup> two crucial regions for small molecule translocation along the transport direction (Z, **Figure 3**) were identified: (i) the preorientation region (PR), (from 5 Å < Z < 10 Å;

**Figure 3)** with R167, R168, and D121 as key motifs allowing the binding of ampicillin and other dipolar molecules;<sup>21,22</sup> (ii) the constriction region (CR) (from  $5 \text{ \AA} < Z < -5 \text{ \AA}$ ; **Figure 3**) whose key motifs are the positively charged residues of the basic ladder (R42, R82, R132, K16) and the negatively charged residues of the constricting loop L3 (D113 and E117).

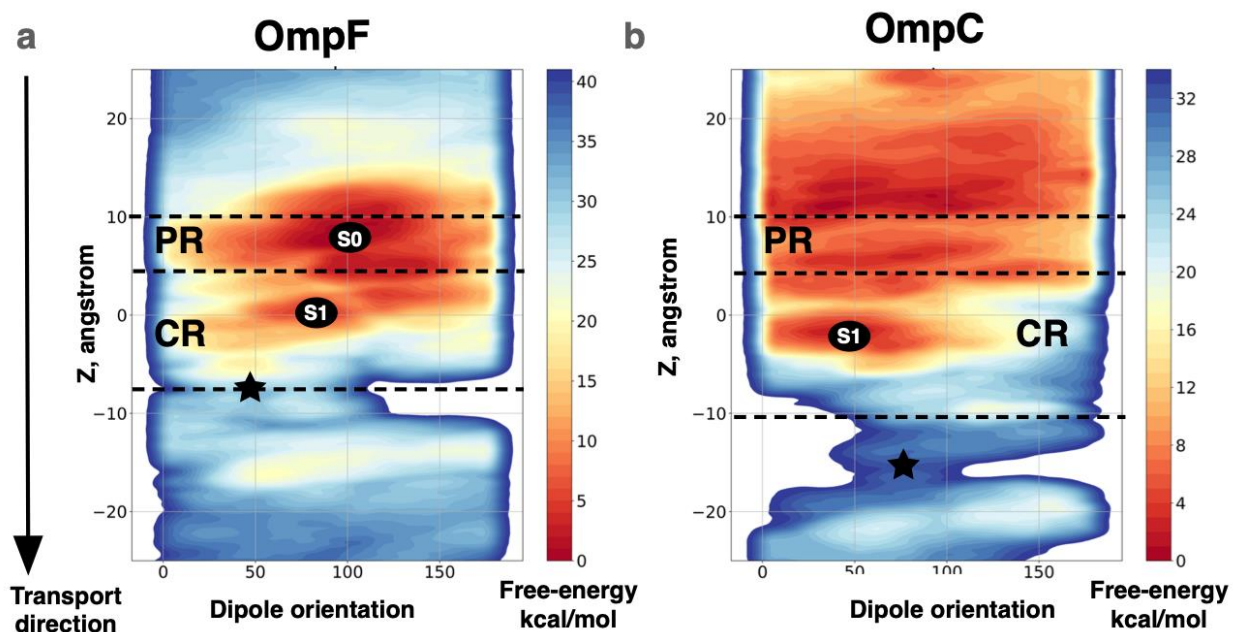


**Figure 3. Kanamycin permeation path through OmpF and OmpC.** Qualitative free energy surface for a single kanamycin translocation event showing the region of main interactions. The relevant conformations for kanamycin transport through OmpF (a) and OmpC (b) are highlighted. The ion current blocking states are highlighted as S1 and the bottleneck for transport (the energetic saddle point) as a star. The key regions for transport are delimited and labelled, e.g. PR (pre-orientation region) and CR (constriction region)

Both regions are characterized by a strong electric field component perpendicular to the axis of diffusion, more intense in the CR than in the PR<sup>20,21</sup> (**Figure S2b**). One striking difference between the porins is that in OmpF the transversal electric field is always higher than that in OmpC,<sup>6</sup> as reported in **Figure S2b**. In the case of kanamycin transport through OmpF, the first deep minimum (**Figure 3a, state S0**) is located in the PR. As it can be observed in **Figure 4 b,c**,

in this position and due to its size ( $71 \text{ \AA}^2$ , **Figure 4a**, and **Table S3**), kanamycin already interacts with two of the negatively charged key motifs of the CR, E117 and D121 of loop L3. Its total dipole moment is aligned to the transversal electric field of the pore (**Figure 4b**); however, kanamycin does not completely block the pore at this position.

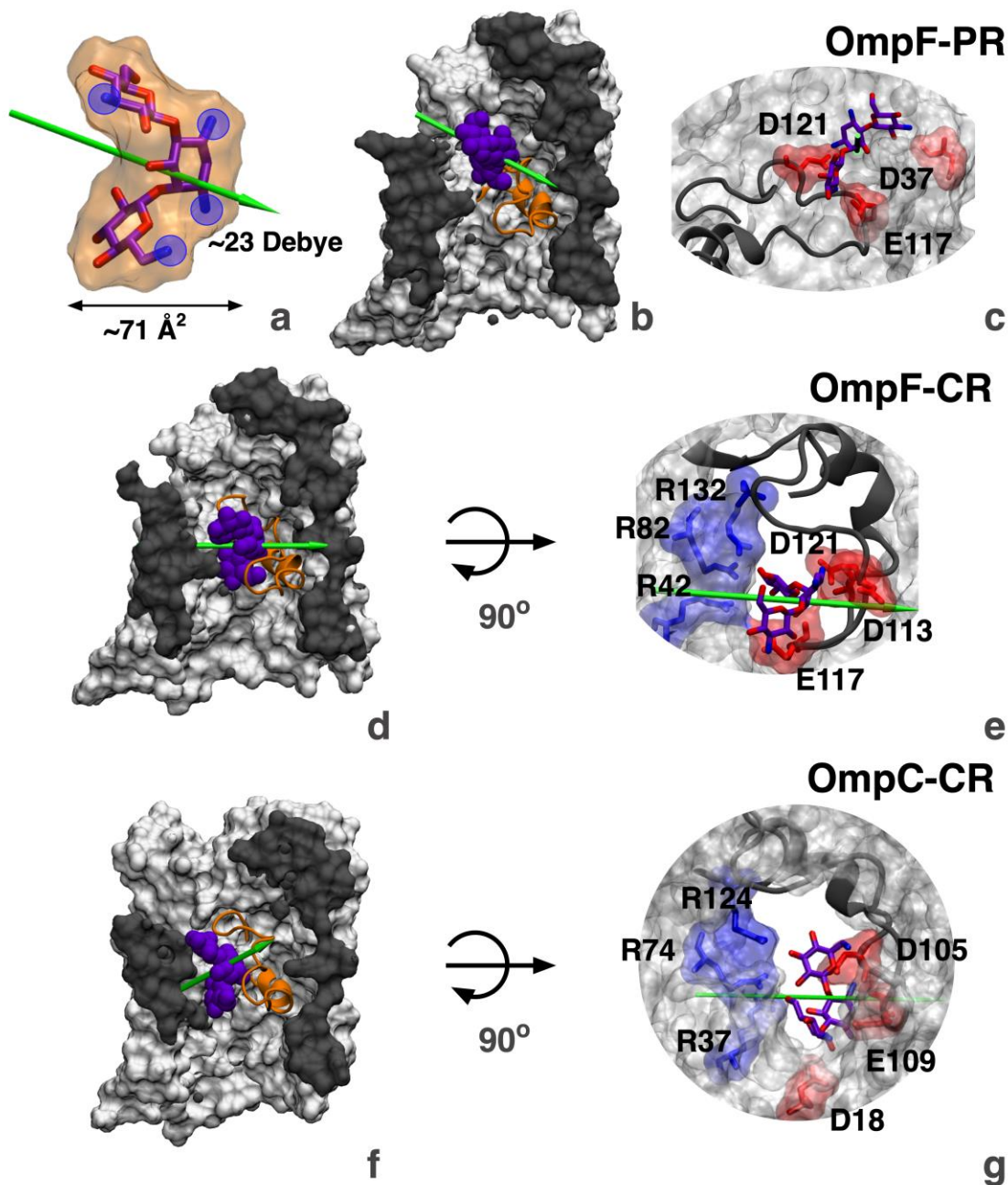


**Figure 4.** Structure of kanamycin and main conformations along the translocation path in OmpF

and OmpC. **a)** Licorice representation of kanamycin with its van der Waals surface superimposed in orange, dipole moment in green and positively charged groups highlighted in blue. Kanamycin (represented as violet van der Waals spheres) position with respect to the main diffusion axis of the pore (partial surface representation) in the main conformations during permeation through OmpF (**b, d**) and OmpC (**f**). Kanamycin interactions with charged groups from the walls of the pore are depicted in licorice for each conformation panels (**c, e, g**).

From this position, kanamycin misaligns its dipole moment in order to approach the CR, attracted by the other two negatively charged motifs of the loop L3, E117 and D113 (**Figure S2, S3 states 2 and 3**). In the second minimum **S1** of **Figure 3**, kanamycin is located in the narrowest region of the CR (**Figure 4d**), again with its dipole moment fully aligned to the transversal electric field. It interacts with all key charged motifs of the eyelet, namely the positively charged arginines R42, R82, R132 and the negatively charged D113, E117 and D121 (**Figure 4e**). As it can be seen now, kanamycin completely blocks the pore. The energetic bottleneck for kanamycin transport is the exit of the CR. As it can be seen from the main interactions in the saddle point conformation, **Figure 3** (saddle-point indicated with a star), the interactions of kanamycin with the charged motifs of the loop L3 are very strong (**Figure S3-state 0**).

In the case of the kanamycin transport through OmpC, fewer steps seem to be relevant in the transport process (**Figure S2(c)**, bottom panel). The capture of kanamycin in OmpC (**Figure 3, Figure S4**) is less pronounced than in OmpF, probably due to the smaller electric field in the preorientation region. Conversely to OmpF, in OmpC kanamycin does not interact with the charged key motifs of the loop L3 when located in the PR, but it interacts mainly with the walls and the loop L2 of the monomer 2 (**Figure S4-states 1-2**). Once inside the CR (**Figure 3b: S1**), kanamycin aligns its dipole moment to the transversal electric field of the pore (**Figure 4f**), interacting with the main charge motifs of the OmpC eyelet, namely the positively charged arginines R37 and R74 and the negatively charged residues of the loop L3 (D105, E109 and

D113). As in OmpF, the main energetic bottleneck is the exit from the CR, due to the strong interactions with its charged motifs (**Figure S4 (state 0)**).

In order to further investigate the two blocking-states identified respectively for OmpF and OmpC, we performed 4 single replica simulations of OmpF/OmpC with kanamycin inside the eyelet and with an applied voltage of -100 mV (**Figure S5**). The four replicas were stable and retained the interactions with the pore for the whole length of the simulation, as it can be observed in Figure S5a. The probability distribution of the distance of the centre of mass of kanamycin to the blocking site in OmpF is centred in  $\sim 1 \text{ \AA} \pm$  (**Figure S5a**, upper panel). We observed that although kanamycin is predicted to block the cation ( $\text{K}^+$ , blue) passage almost completely, on average 1  $\text{K}^+$  translocates compared to 33  $\text{K}^+$  in the empty trimer (**Figure S5b**, upper panel, and **Table S2**); it does not blocks anions ( $\text{Cl}^-$ , red), instead it is predicted to enhance their passage, as we have 8  $\text{Cl}^-$  on average that can pass compared to 5 in the empty trimer (**Figure S5b**, upper panel, and **Table S2**). The same is predicted with OmpC: the presence of kanamycin in the CR blocks partially the passage of cations (on average 3 $\text{K}^+$  versus 39  $\text{K}^+$  in the empty trimer, **Figure S5b** and **Table S2**), while it somehow enhances the flux of anions, as on average 15  $\text{Cl}^-$  translocate in the presence of kanamycin, while in the empty trimer 3  $\text{Cl}^-$  go through (**Figure S5b**, lower panel, and **Table S2**).

### Whole-cell assays

The experiments with purified proteins as well as the numerical simulations indicated permeation of kanamycin through both major porins OmpF and OmpC. To validate the relevance of these observations in bacterial cells, we determined the kanamycin susceptibility of different porin mutants. We employed the single-gene deletion mutants of *ompF* and *ompC* from the Keio

collection and generated in the current study a double deletion strain missing both of these major porin genes<sup>23</sup>. Kanamycin susceptibility was measured by a standard assay for the determination of the minimal inhibitory concentration (MIC) according to guidelines as well as by streaking of the *E. coli* strains on an agar plate containing a linear kanamycin gradient. *E. coli* missing either *ompF* or *ompC* alone (single knockout strains) showed similar susceptibility to kanamycin as the wild type parent strain *E. coli* BW25113 (**Figure 5**). However, the double deletion strain *E. coli*  $\Delta ompF\Delta ompC$  showed a clear and statistically significant decrease in kanamycin susceptibility. This result indicates that kanamycin is able to use both porins, *ompF* as well as *ompC* for outer membrane translocation and that a single deletion of either porin still leaves the other available. Similar observations were made with the further aminoglycosides paromomycin, amikacin and gentamicin (Figures S6 & S7) and data for aminoglycosides were compared to  $\beta$ -lactams and fluoroquinolones, representatives of which were previously shown to pass through OmpF and OmpC (Figure S8 & Table S4). Importantly, although the susceptibility to aminoglycosides was clearly and reproducibly decreased in the  $\Delta ompF\Delta ompC$  double knockout strain, the absolute value of the MIC increased only about 2-fold. This finding indicates that at least one further translocation mechanism, such as self-promoted uptake<sup>9</sup> and/or one or more further porin(s), is still available for the AGs as option to cross the OM of *E. coli*.

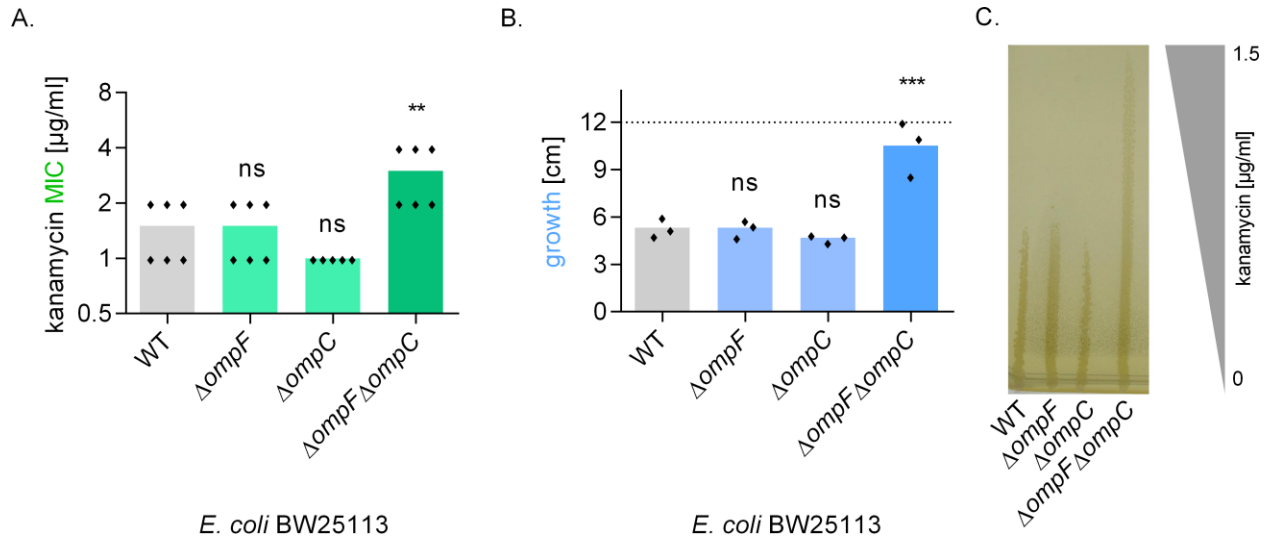


**Figure 5.** The role of porins in kanamycin susceptibility of *E. coli* BW25113. A) The kanamycin MIC is significantly increased when both major porin genes *ompF* and *ompC* are deleted, while single porin knockout strains did not show increased resistance. MIC values are represented on a logarithmic scale. B, C) The same trend could be observed when *E. coli* porin mutant strains were streaked on agar plates with a linear kanamycin gradient. The dotted line represents the maximal length of the plate. One representative biological replicate of B is shown in C. Each diamond represents one independent measurement from a different day. The vertical colored bars show the arithmetic mean of all data points. Statistical analysis was done using unpaired Student's *t*-test with Holm-Bonferroni correction, comparing the mutants to the wildtype (WT) strain. not significant (ns),  $P > 0.05$ ; \*\*,  $P \leq 0.01$ ; \*\*\*,  $P \leq 0.001$ .

## DISCUSSION

The combination of two independent experimental techniques and molecular dynamics simulations showed that kanamycin can translocate through OmpF and OmpC, but not through OmpN. In both OmpF and OmpC, kanamycin shows strong interactions with the pore wall, especially with the anionic residues of the loop L3, due to its positive charge. Further, the orientation of its dipole, transversal to the long axis of the molecule itself (**Figure 4a**) allows the accommodation of kanamycin in the pore with its long axis parallel to the axis of diffusion and, at the same time, with the dipole aligned to the transversal electric field (**Figure 4 d,e,f,g**). From a structural point of view, kanamycin adapts perfectly to the geometry of the pore and its electrostatics. The negative electrostatic potential inside both OmpF and OmpC<sup>6</sup> creates the

condition for quite strong binding of cationic molecules such as kanamycin, as shown from the current traces in **Figure 2** and simulations data in **Figure 3 and Figure 4**. This is not the case for OmpN. Though more selective for small cations ( $K^+$ ), it has a pore not compatible with the dimension of kanamycin (the minimal pore radius is smaller than 1 Å, as it can be estimated from comparison of the  $K_2SO_4$  conductivity for all the pores, see **Table S1**). The reversal potential method confirms that no translocation events occur in OmpN (**Table 1**).

It is worth to note that kanamycin has an average minimal projection area of 71 Å<sup>2</sup> (see **Table S3**). Among small-molecule antibiotics presented in a recent database,<sup>24</sup> only ceftazidime and piperacillin show the size comparable to kanamycin, respectively, 68 Å<sup>2</sup> and 77 Å<sup>2</sup>, while all the other antibiotics have the minimal projection area that does not exceed 60 Å<sup>2</sup> (see **Table S3**). Interestingly, both ceftazidime and piperacillin are anionic, so they are not favoured to translocate through negatively charged OmpF and OmpC. However, ceftazidime has been shown to translocate through OmpF and with low numbers through OmpC,<sup>25</sup> while the larger piperacillin showed extremely low permeability through both of them.<sup>6</sup> In our study we observed a low MIC increase for ceftazidime and none at all for piperacillin upon *ompF* and *ompC* double deletion (see Figure S8 and Table S4). Kanamycin, larger than ceftazidime, can go through OmpF and OmpC with comparable numbers thanks to a larger dipole moment, especially for the transverse component (**Table S3**). This is the electrostatic compensation of the steric barrier.

The simulations of the translocation of kanamycin through OmpF showed the existence of an additional binding site in the pre-orientation region (**Figure 4b,c**), exactly where the dipolar and zwitterionic ampicillin and norfloxacin showed strong interactions.<sup>21,22</sup> In this conformation, kanamycin's dipole can be aligned along the transversal electric field. However, due to the relatively large pore size there, there is no complete blockage of the passage of the small ions.

This correlate with the presence of two different conduction levels in OmpF, see histogram on Figure 1A. This second site works also as a reservoir, accumulating kanamycin from the solvent, thus causing the saturation seen in **Figure 2A**.

The insights from these biophysical and computational experiments could be transferred to and confirmed in living *E. coli* cells. *E. coli* mutants, lacking one or both major porins, were exposed to kanamycin in different experimental setups and a resistance phenotype emerged, when OmpF and OmpC were missing in parallel (**Figure 5**). Previous investigations on the role of OmpF and OmpC in kanamycin resistance had been contradictory. In an early publication, the OmpF-deficient strain *E. coli* JF703 displayed increased kanamycin resistance.<sup>11</sup> However, this strain was also polymyxin B-resistant,<sup>11</sup> suggesting that it might carry further mutations besides that of *ompF*. In a later study, no effects on kanamycin MICs could be observed for *E. coli* single mutants of *ompF* and *ompC* or in a regulator mutant lacking both porins<sup>9</sup>. In the current study, we constructed a markerless *ompF ompC* double knockout strain, and compared it to its isogenic wildtype and both markerless single knockout strains, using two different antimicrobial assay read-outs and conducting multiple experimental repetitions for statistical validation. While we corroborate that a single deletion of either *ompF* or *ompC* does not change the susceptibility of *E. coli* to different AGs, the double deletion of both major porins reduces susceptibility by a factor of two. This finding indicates, on the one hand that both porins contribute to AG uptake in *E. coli* and on the other had it demonstrates that their impact is rather limited. Besides OmpF and OmpC, AGs have further means of entering *E. coli*. Still another porin could potentially be involved, it is also widely accepted that the polycationic AGs displace divalent cations from the LPS molecules, thereby forcing their passage across the destabilized outer membrane by self-promoted uptake.<sup>26-28</sup> The concept that AGs have multiple and independent means of crossing

the outer membrane is reflected by the fact that uptake mutations are not the focus of clinical resistance development. Indeed, AG resistance is mostly based on acquired and plasmid-transferable AG-modifying enzymes or 16S rRNA methyltransferases.<sup>29</sup>

Besides, we determined additional MIC values for a number of antibiotics from different classes (see Figure S8 and Table S4). Several factors contribute to the MIC value (e.g. target affinity, efflux, porin-mediated and additional porin-unrelated uptake routes, environmental conditions). Although antibacterial agents are often grouped within the same antibiotic class according to a related pharmacophore and corresponding mode of action, they are different structural entities that are influenced by the range of these factors to a different extent. Interestingly, the change in MIC upon porin deletion of AG is in the range found for some cephalosporins and penicillins (e.g. ceftazidime, ceftriaxone, carbenicillin). In addition, kanamycin needs further translocation across the inner cell membrane to reach its target. Despite the relatively low flux value, the periplasmic space might be rapidly equilibrated and the passage through both porins has only a small effect on the activity.

Inspection of previous investigations on concentration driven flux through OmpF at a 10  $\mu$ M gradient revealed 600 molecules/s for avibactam,<sup>30</sup> 350 molecules/s for cefotaxime (unpublished), 240 molecules/s for ampicillin,<sup>31</sup> and 10 – 20 molecules/s of kanamycin, but also substantially lower values for cefepime<sup>32</sup> (0.035 molecules/s, extrapolated from on-rates, without counting fast events<sup>33</sup>). These expected fluxes will enter the periplasm of bacteria. To estimate the number of molecules after equilibration inside bacteria, if we assume a sphere with a radius of 1  $\mu$ m size mostly filled by biomass. This may allow for a few thousand antibiotics at 10  $\mu$ M. Assuming further a few hundreds to thousands of channels, the concentration equilibrium will be easily achieved within a few seconds also for kanamycin. Other techniques based on single cell

fluorescence using fluoroquinolones or mass spectrometry determined that the equilibrium between the inner and the outer concentration occurs within a few minutes.<sup>5,34,35</sup> Porins are the limiting factors for the efficacy of an antibiotic either (i) when there are not alternative uptake pathways and the number of porins is low, or (ii) when the rate of entry is very low. In the case of kanamycin, two highly abundant porins are used and further uptake routes (i.e. self-promoted uptake) contribute in addition.

## CONCLUSIONS

Although aminoglycosides are a mainstay of clinical anti-Gram-negative therapy, their molecular uptake mechanism has remained a matter of debate. In our interdisciplinary study we tackled the problem by a complementary biophysical, computational and microbiological approach and demonstrate the involvement of the porins OmpF and OmpC in kanamycin translocation across the OM on three different levels: the reconstituted proteins, pore structure and growing bacterial cells. By describing and quantifying the transport of kanamycin through three different pores, with increasing size (OmpN, OmpC, OmpF) and with inverted increased selectivity to small cations, we were able to investigate the role of the steric term and the electrostatic compensation. In OmpN, the small open pore does not allow the translocation. In OmpC, the higher negative charge compared to OmpF is enough to compensate for the smaller size. Finally, the largest pore, OmpF, shows reduced flux due to the presence of an additional binding site near the mouth of the channel. This example provides a clear picture of optimal transport through a size-constricted pore combining electrostatic compensation of a steric barrier. Kanamycin with its cylindrical shape can fit perfectly well into the constriction region. At the same time, the position of the four positively charged groups provides a dipole that can align to

the transversal electric field, thus, allowing a binding near the constriction region and compensating the steric barrier while translocating. Eventually, about 10 - 20 kanamycin molecules per second can permeate through OmpF and OmpC under a 10  $\mu$ M concentration gradient, and whole-cell studies provided evidence that translocation of kanamycin *via* porins is relevant for antibiotic potency, though other uptake mechanisms are not excluded.

## **METHODS**

### **Materials**

Kanamycin sulphate and cefoxitin sodium salt were obtained from Carl Roth (Mannheim, Germany), gentamicin sulphate from AppliChem PanReac (Darmstadt, Germany), paromomycin sulphate from Cayman Chemical (Michigan, U.S.A.), amikacin disulphate from Acros Organics (Geel, Belgium) potassium sulphate salt was obtained from Sigma-Aldrich (Dorset, United Kingdom), 1,2-diphytanoyl-sn-glycero-3-phosphocoline was purchased from Avanti Polar Lipids (Alabaster, AL) and all other chemicals used were procured from AppliChem. The proteins were produced in house following previous publications<sup>18</sup> and SI.

### **Planar lipid bilayer and electrical recording. Single and Multi-Channel Measurements:**

Single channel recording apparatus consisted of a two-compartment Teflon chamber (~ 2.5 mL each) separated by a 25  $\mu$ m thick Teflon partition with an aperture of  $\approx$ 100  $\mu$ m diameter for membrane formation. Bilayer lipid membranes were formed from 1,2-diphytanoyl-sn-glycero-3-phosphocholine (DPhPC) using the monolayer opposition technique.<sup>36</sup> The aperture was pre-treated with a hexadecane/hexane solution (1 % v/v) and was allowed to cure for ~ 20 mins to achieve solvent evaporation. The *trans*- and *cis*-sides of the chambers were filled with buffer solution, 1 M KCl, 10 mM HEPES at pH 7.0. 10  $\mu$ l of lipid in pentane (5 mg/ml) was added to both sides of the chamber, and a bilayer was formed after evaporation of pentane. Single channel reconstitution was achieved by addition of purified OmpF or OmpC porins into the *cis*-side of the chamber at a volume of  $\approx$ 0.3  $\mu$ l from their stock solutions (1 mg/ml) and diluted by ~100 fold

using Genapol X-080 (1 % v/v). The final protein concentration in the chamber was  $\approx 1$   $\mu$ M. Channel current traces were recorded with Ag/AgCl pellet electrodes (World Precision Instruments), the *cis* side of the chamber being the virtual ground, using the Axopatch 200B (Molecular Devices, LLC) patch-clamp amplifier in V-clamp mode (whole cell  $\beta = 1$ ) with a CV-203BU headstage. The output signal was filtered by a lowpass Bessel filter at 10 kHz and saved at a sampling frequency of 50 kHz using an Axon Digidata 1440A digitizer (Molecular Devices, LLC). Data analysis was performed with an in-house analysis suite created with the LabVIEW software suite (National Instruments).

Further, for measuring the electrophysiological reversal potential assay (Multi channel) for asymmetric condition we used commercial calomel electrodes (Metrohm). The *cis* side electrode of the cell was grounded, whereas the *trans* side electrode was linked to the headstage of an Axopatch 200B amplifier in the voltage clamp mode. Signals were filtered by an on-board low pass Bessel filter at 10 kHz with a sampling frequency of 50 kHz. Analysis of the current recordings was completed using Clampfit (Axon Instruments). The relative permeability of cations vs solute anions in the bi-ionic case ( $P_{Kanamycin^{4+}}/P_{sulphate^{2-}}$ ) were obtained by fitting of the experimental I-V-curves with the Goldman-Hodgkin-Katz current equation.<sup>37</sup> The flux was estimated using the permeability ratios between the cation over anion flux and an estimation of the ion current induced by a reversal potential.<sup>12,13,37</sup>

### **All-atom molecular dynamics simulations**

The experimental X-ray structures of OmpF and OmpC (PDB Id: 2OMF, 2J1N) were used as starting coordinates for molecular dynamics (MD) simulations. All the amino acid residues were simulated in the ionization state at neutral pH except for the E296 (OmpF) and D299 (OmpC) which were protonated (net charge 0) as suggested by Varma et al.<sup>38</sup> For both systems the entire trimer was embedded in a pre-equilibrated POPC (1-palmitoyl-2-oleoyl-sn-glycero-3-phosphocholine) bilayer of 259 lipids. The system was oriented in order to centre the protein at the origin of the coordinate system and align the channel along the z-axis (positive z: extracellular side; negative z: periplasmic side). Thus, we solvated it in a 150 mM KCl solution. The selected force fields were: AMBER14SB<sup>39</sup> for the protein, AMBER lipid14<sup>40</sup> for the POPC

molecules, TIP3P<sup>41</sup> for water. After 1 ps of energy minimization (conjugate gradients), a slow heating from 10 to 300 K was carried out for 1 ns. During this stage, positional restraints were applied on the protein  $\alpha$ -carbons (all three dimensions) as well as on the lipids phosphorus atoms (along z only). After releasing the constraints on the POPC, an equilibration stage follows for 4 ns in the NPT ensemble at 1.0 bar and 300 K. Finally, 0.6 microseconds MD simulations were performed in the NVT ensemble after the elimination of the protein restraints. The NPT equilibration was performed with the program NAMD,<sup>42</sup> with 1.0 fs time-step, and treating long-range electrostatics with the soft particle mesh Ewald (SPME) method (64 grid points and order 4 with direct cutoff at 1.0 nm and 1.0 Å grid-size). Pressure control was applied using the Nose-Hoover method (extended Lagrangian) with isotropic cell, integrated with the Langevin Dynamics (200 fs and 100 fs of piston period and decay, respectively). The latter was also applied for temperature control with 200 fs thermostat damping time. Production run in the NVT ensemble with a time step of 4 fs was performed through the ACEMD code<sup>43</sup> compiled for GPUs. The Langevin thermostat was used with 1 ps damping time. SPME was used to treat the electrostatics as for the equilibration stage.

The GAFF force-field parameters<sup>44</sup> were used to describe kanamycin (PubChem: CID 6032). Partial atomic charges were evaluated according to the RESP approach:<sup>45</sup> the molecule was first optimized at the HF/6-31G(d) level, up to a convergence in energy of  $10^{-5}$  au, using the Gaussian03 package.<sup>46</sup> Atomic RESP charges were derived from the electrostatic potential using the antechamber module of the AMBER package.<sup>47</sup> The minimal projection area and the charge at different pH were calculated with the software Marvin.<sup>48</sup>

Starting from the final configuration of the OmpF and OmpC simulation described above, the molecule was placed outside the lumen of the first monomer. The difference between the z-coordinate of the centre of mass (COM) of the antibiotic and the z-coordinate of the com of the protein monomer was 32 Å. A thousand steps of energy minimization were performed. The equilibration stage followed for 1 ns in the NVT ensemble at 300 K as described hereinbefore. Well-tempered metadynamics<sup>49,50</sup> simulation were performed with the ACEMD code<sup>43</sup> combined with PLUMED,<sup>51</sup> until the first effective translocation through the protein constriction region (CR) was observed. Two biased collective variables were used, namely, the antibiotic position and the projection of the dipole moment of the antibiotic onto the z-axis of the channel. In practice, the 'position'  $\Delta z$  was defined as the difference of the z-coordinate between the COM of

the antibiotic and that of the porin first monomer. During the metadynamics run, energy biases were added every 50 ps to each collective variable (height 0.1 au;  $\sigma$  0.25 and 5.0 au for position and dipole moment, respectively) with a bias factor of 10.0, to ensure the slow exploration of the translocation event. For the two cation-blocking conformations, 4 replicas of 100 ns were launched with an applied potential of -100 mV to evaluate ion current in presence of kanamycin.

### **Determination of the aminoglycoside sensitivity of *E. coli* porin mutants**

Minimal inhibitory concentrations (MIC) of aminoglycosides were determined according to guidelines of the Clinical Laboratory Standards Institute (CLSI)<sup>52</sup> using cation-adjusted Mueller Hinton broth (MHBII). Strains used in this work are listed in **Table S5**. Bacterial cell numbers were adjusted to an inoculum of  $5 \times 10^5$  cells/ml and the lowest concentration to inhibit visible bacterial growth was determined after 18 h of incubation at 37 °C. For agar gradient plates, 7.5 g/l of agar-agar was added to the broth. The first layer was poured without kanamycin and was solidified while the plate was at an inclined position. The top layer containing kanamycin at a concentration of 1.5  $\mu$ g/ml was solidified when the plate was level. Prior to use the plate was stored over night at 4 °C. *E. coli* cells were suspended in 0.9 % NaCl (w/v) and the optical density at 600 nm ( $OD_{600}$ ) was adjusted to 0.1. This cell suspension was streaked on the agar gradient plates using cotton swabs and growth was read after 18 h of incubation at 37 °C. Statistical analysis was performed using R (the R foundation for Statistical Computing, version 3.6.1). Unpaired Student's t-test was used so determine statistical significance. For multiple comparisons, alpha was adjusted with the Holm-Bonferroni method.

### **Generation of gene deletion strains**

Porin gene deletions were performed as described by Datsenko & Wanner.<sup>53</sup> Briefly, the kanamycin resistance cassette was amplified from the vector pKD13, using primers (**Table S6**) attached to homologous ends of the porin genes of interest. *E. coli* cells were first transformed with the helper plasmid pKD46 and in a second transformation round with the constructed PCR products. The resistance cassette was removed with the helper plasmid pCP20. Gene deletions were confirmed by PCR.

## **AUTHOR INFORMATION**

### **Author Contributions**

The manuscript was written through contributions of all authors. All authors have given approval to the final version of the manuscript. ‡These authors contributed equally.

### *Corresponding Authors*

\*Matteo Ceccarelli, Department of Physics and IOM/CNR, University of Cagliari, 09042

Monserrato, Italy, [matteo.ceccarelli@dsf.unica.it](mailto:matteo.ceccarelli@dsf.unica.it)

\* Mathias Winterhalter, Jacobs University, D-28719 Bremen, Germany,

[M.Winterhalter@jacobs-university.de](mailto:M.Winterhalter@jacobs-university.de)

\* Heike Brötz-Oesterhelt, Department of Microbial Bioactive Compounds, Interfaculty Institute of Microbiology and Infection Medicine, University of Tübingen, D-72076 Tübingen, Germany, and German Center for Infection Research (DZIF), partner site D-72076 Tübingen, [heike.broetz-oesterhelt@uni-tuebingen.de](mailto:heike.broetz-oesterhelt@uni-tuebingen.de)

## **ASSOCIATED CONTENT**

### **Supporting Information**

The Supporting Information is available free of charge on the ACS Publications website. PDF file with 8 Figures, S1-S8 and 7 Tables, S1-S7.

### **Funding Sources**

The research leading to these results was conducted as part of the Translocation consortium ([www.translocation.eu](http://www.translocation.eu)) and has received support from the Innovative Medicines Initiative Joint Undertaking under Grant Agreement no. 115525, resources which are composed of financial contribution from European Union's seventh framework programme (FP7/2007-2013) and EFPIA companies. H.B-O., D.H. and A.B. gratefully acknowledge funding by the German Center of Infection Research (DZIF), project TTU 09.819, and infrastructural support by the Deutsche Forschungsgemeinschaft (DFG, German Research Foundation) under Germany's Excellence Strategy – EXC 2124 – 390838134. M.C. would like to thank the partial funding from MIUR “Progetti di Ricerca di Interesse Nazionale” (2015795S5W).

## Notes

### ABBREVIATIONS

OM: Outer Membrane; LPS: lipopolysaccharides; AG: aminoglycosides; COM: center of mass; GHK: Goldman-Hodgkin-Katz; PR: preorientation region; CR: constriction region; MIC: minimal inhibitory concentration; WT: wildtype; MD: molecular dynamics; SPME: soft particle mesh Ewald.

## REFERENCES

- (1) Nikaido, H. Molecular Basis of Bacterial Outer Membrane Permeability Revisited. *Microbiol. Mol. Biol. Rev.* **2003**, *67*, 593–656.
- (2) Richter, M. F.; Drown, B. S.; Riley, A. P.; Garcia, A.; Shirai, T.; Svec, R. L.; Hergenrother, P. J. Predictive Compound Accumulation Rules Yield a Broad-Spectrum Antibiotic. *Nature* **2017**, *545*, 299–304.
- (3) Vergalli, J.; Bodrenko, I. V.; Masi, M.; Moynié, L.; Acosta-Gutiérrez, S.; Naismith, J. H.; Davin-Regli, A.; Ceccarelli, M.; van den Berg, B.; Winterhalter, M.; Pagès, J.-M. Porins and Small-Molecule Translocation across the Outer Membrane of Gram-Negative Bacteria. *Nat. Rev. Microbiol.* **2020**, *18*, 164–176.
- (4) Nakae, T. Identification of the Outer Membrane Protein of E.Coli That Produces Transmembrane Channels in Reconstituted Vesicle Membranes. *Biochem. Biophys. Res. Commun.* **1976**, *71*, 877–884.
- (5) Ruggiu, F.; Yang, S.; Simmons, R. L.; Casarez, A.; Jones, A. K.; Li, C.; Jansen, J. M.; Moser, H. E.; Dean, C. R.; Reck, F.; Lindvall, M. Size Matters and How You Measure It: A Gram-Negative Antibacterial Example Exceeding Typical Molecular Weight Limits. *ACS Infect. Dis.* **2019**, *5*, 1688–1692.
- (6) Acosta-Gutiérrez, S.; Ferrara, L.; Pathania, M.; Masi, M.; Wang, J.; Bodrenko, I.; Zahn, M.; Winterhalter, M.; Stavenger, R. A.; Pagès, J.-M.; Naismith, J. H.; van den Berg, B.; Page, M. G. P.; Ceccarelli, M. Getting Drugs into Gram-Negative Bacteria: Rational Rules for Permeation through General Porins. *ACS Infect. Dis.* **2018**, *4*, 1487–1498.

- (7) Lou, H.; Chen, M.; Black, S. S.; Bushell, S. R.; Ceccarelli, M.; Mach, T.; Beis, K.; Low, A. S.; Bamford, V. A.; Booth, I. R.; Bayley, H.; Naismith, J. H. Altered Antibiotic Transport in OmpC Mutants Isolated from a Series of Clinical Strains of Multi-Drug Resistant E. Coli. *PLoS One* **2011**, *6*, e25825.
- (8) Pagès, J.-M.; James, C. E.; Winterhalter, M. The Porin and the Permeating Antibiotic: A Selective Diffusion Barrier in Gram-Negative Bacteria. *Nat. Rev. Microbiol.* **2008**, *6*, 893–903.
- (9) Hancock, R. E. W.; Farmer, S. W.; Li, Z. S.; Poole, K. Interaction of Aminoglycosides with the Outer Membranes and Purified Lipopolysaccharide and OmpF Porin of Escherichia Coli. *Antimicrob. Agents Chemother.* **1991**, *35*, 1309–1314.
- (10) Nakae, R.; Nakae, T. Diffusion of Aminoglycoside Antibiotics across the Outer Membrane of Escherichia Coli. *Antimicrob. Agents Chemother.* **1982**, *22*, 554–559.
- (11) Foulds, J.; Chai, T. J. New Major Outer Membrane Proteins Found in an Escherichia Coli TolF Mutant Resistant to Bacteriophage TuIb. *J. Bacteriol.* **1978**, *133*, 1478–1483.
- (12) Ghai, I.; Pira, A.; Scorciapino, M. A.; Bodrenko, I.; Benier, L.; Ceccarelli, M.; Winterhalter, M.; Wagner, R. General Method to Determine the Flux of Charged Molecules through Nanopores Applied to  $\beta$ -Lactamase Inhibitors and OmpF. *J. Phys. Chem. Lett.* **2017**, *8*, 1295–1301.
- (13) Ghai, I.; Winterhalter, M.; Wagner, R. Probing Transport of Charged  $\beta$ -Lactamase Inhibitors through OmpC, a Membrane Channel from E. Coli. *Biochem. Biophys. Res. Commun.* **2017**, *484*, 51–55.

- (14) Eaton, D. C. Ionic Channels of Excitable Membranes. Bertil Hille. Sunderland, Ma: Sinauer Associates, 1984. *J. Neurosci. Res.* **1985**, *13*, 599–600.
- (15) Nikaido, H.; Vaara, M. Molecular Basis of Bacterial Outer Membrane Permeability. *Microbiol. Rev.* **1985**, *49*, 1–32.
- (16) Prilipov, A.; Phale, P. S.; Koebnik, R.; Widmer, C.; Rosenbusch, J. P. Identification and Characterization of Two Quiescent Porin Genes, NmpC and OmpN, in Escherichia Coli BE. *J. Bacteriol.* **1998**, *180*, 3388–3392.
- (17) Mahendran, K. R.; Hajjar, E.; Mach, T.; Lovelle, M.; Kumar, A.; Sousa, I.; Spiga, E.; Weingart, H.; Gameiro, P.; Winterhalter, M.; Ceccarelli, M. Molecular Basis of Enrofloxacin Translocation through OmpF, an Outer Membrane Channel of Escherichia Coli - When Binding Does Not Imply Translocation. *J. Phys. Chem. B* **2010**, *114*, 5170–5179.
- (18) Lamichhane, U.; Islam, T.; Prasad, S.; Weingart, H.; Mahendran, K. R.; Winterhalter, M. Peptide Translocation through the Mesoscopic Channel: Binding Kinetics at the Single Molecule Level. *Eur. Biophys. J.* **2013**, *42*, 363–369.
- (19) Acosta-Gutierrez, S.; Scorciapino, M. A.; Bodrenko, I.; Ceccarelli, M. Filtering with Electric Field: The Case of E. Coli Porins. *J. Phys. Chem. Lett.* **2015**, *6*, 1807–1812.
- (20) Gutiérrez, S. A.; Bodrenko, I.; Scorciapino, M. A.; Ceccarelli, M. Macroscopic Electric Field inside Water-Filled Biological Nanopores. *Phys. Chem. Chem. Phys.* **2016**, *18*, 8855–8864.
- (21) Bajaj, H.; Acosta Gutierrez, S.; Bodrenko, I.; Mallocci, G.; Scorciapino, M. A.;

- Winterhalter, M.; Ceccarelli, M. Bacterial Outer Membrane Porins as Electrostatic Nanosieves: Exploring Transport Rules of Small Polar Molecules. *ACS Nano* **2017**, *11*, 5465–5473.
- (22) Ziervogel, B. K.; Roux, B. The Binding of Antibiotics in OmpF Porin. *Structure* **2013**, *21*, 76–87.
- (23) Baba, T.; Ara, T.; Hasegawa, M.; Takai, Y.; Okumura, Y.; Baba, M.; Datsenko, K. A.; Tomita, M.; Wanner, B. L.; Mori, H. Construction of Escherichia Coli K-12 In-frame, Single-gene Knockout Mutants: The Keio Collection. *Mol. Syst. Biol.* **2006**, *2*, 2006.0008.
- (24) Mallocci, G.; Vargiu, A.; Serra, G.; Bosin, A.; Ruggerone, P.; Ceccarelli, M. A Database of Force-Field Parameters, Dynamics, and Properties of Antimicrobial Compounds. *Molecules* **2015**, *20*, 13997–14021.
- (25) Allam, A.; Maigre, L.; Vergalli, J.; Dumont, E.; Cinquin, B.; Alves de Sousa, R.; Pajovic, J.; Pinet, E.; Smith, N.; Herbeuval, J.-P.; Réfrégiers, M.; Artaud, I.; Pagès, J.-M. Microspectrofluorimetry to Dissect the Permeation of Ceftazidime in Gram-Negative Bacteria. *Sci. Rep.* **2017**, *7*, 986.
- (26) Mingeot-Leclercq, M. P.; Glupczynski, Y.; Tulkens, P. M. Aminoglycosides: Activity and Resistance. *Antimicrob. Agents Chemother.* **1999**, *43*, 727–737.
- (27) Serio, A. W.; Keepers, T.; Andrews, L.; Krause, K. M. Aminoglycoside Revival: Review of a Historically Important Class of Antimicrobials Undergoing Rejuvenation. *EcoSal Plus* **2018**, *8*, 0002–2018.
- (28) Richter, M. F.; Hergenrother, P. J. The Challenge of Converting Gram-Positive-Only

- Compounds into Broad-Spectrum Antibiotics. *Ann. N. Y. Acad. Sci.* **2019**, *1435*, 18–38.
- (29) Garneau-Tsodikova, S.; Labby, K. J. Mechanisms of Resistance to Aminoglycoside Antibiotics: Overview and Perspectives. *Medchemcomm* **2016**, *7*, 11–27.
- (30) Ghai, I.; Pira, A.; Scorciapino, M. A.; Bodrenko, I.; Benier, L.; Ceccarelli, M.; Winterhalter, M.; Wagner, R. A General Method to Determine the Flux of Charged Molecules Through Nanopores Applied to SS-Lactamase Inhibitors and OmpF. *J. Phys. Chem. Lett.* **2017**, *8*, 1295–1310.
- (31) Ghai, I.; Bajaj, H.; Bafna, J. A.; Hussein, H. A. E. D.; Winterhalter, M.; Wagner, R. Ampicillin Permeation across OmpF, the Major Outer-Membrane Channel in Escherichia Coli. *J. Biol. Chem.* **2018**, *293*, 7030–7037.
- (32) Mahendran, K. R.; Kreir, M.; Weingart, H.; Fertig, N.; Winterhalter, M. Permeation of Antibiotics through Escherichia Coli OmpF and OmpC Porins: Screening for Influx on a Single-Molecule Level. *J. Biomol. Screen.* **2010**, *15*, 302–307.
- (33) Bodrenko, I. V.; Wang, J.; Salis, S.; Winterhalter, M.; Ceccarelli, M. Sensing Single Molecule Penetration into Nanopores: Pushing the Time Resolution to the Diffusion Limit. *ACS Sensors* **2017**.
- (34) Dumont, E.; Vergalli, J.; Conraux, L.; Taillier, C.; Vassort, A.; Pajović, J.; Réfrégiers, M.; Mourez, M.; Pagès, J.-M. Antibiotics and Efflux: Combined Spectrofluorimetry and Mass Spectrometry to Evaluate the Involvement of Concentration and Efflux Activity in Antibiotic Intracellular Accumulation. *J. Antimicrob. Chemother.* **2018**, *74*, 58–65.
- (35) Reck, F.; Jansen, J. M.; Moser, H. E. Challenges of Antibacterial Drug Discovery. *Arkivoc*

**2019**, *2019*, 227–244.

- (36) Montal, M.; Mueller, P. Formation of Bimolecular Membranes from Lipid Monolayers and a Study of Their Electrical Properties. *Proc. Natl. Acad. Sci.* **1972**, *69*, 3561–3566.
- (37) Sullivan, H. Ionic Channels of Excitable Membranes, 2nd Ed. *Neurology* **1992**, *42*, 1439–1439.
- (38) Varma, S.; Chiu, S. W.; Jakobsson, E. The Influence of Amino Acid Protonation States on Molecular Dynamics Simulations of the Bacterial Porin OmpF. *Biophys. J.* **2006**, *90*, 112–123.
- (39) Maier, J. A.; Martinez, C.; Kasavajhala, K.; Wickstrom, L.; Hauser, K. E.; Simmerling, C. Ff14SB: Improving the Accuracy of Protein Side Chain and Backbone Parameters from Ff99SB. *J. Chem. Theory Comput.* **2015**, *11*, 3696–3713.
- (40) Dickson, C. J.; Madej, B. D.; Skjevik, Å. A.; Betz, R. M.; Teigen, K.; Gould, I. R.; Walker, R. C. Lipid14: The Amber Lipid Force Field. *J. Chem. Theory Comput.* **2014**, *10*, 865–879.
- (41) Jorgensen, W. L.; Chandrasekhar, J.; Madura, J. D.; Impey, R. W.; Klein, M. L. Comparison of Simple Potential Functions for Simulating Liquid Water. *J. Chem. Phys.* **1983**, *79*, 926–935.
- (42) Phillips, J. C.; Braun, R.; Wang, W.; Gumbart, J.; Tajkhorshid, E.; Villa, E.; Chipot, C.; Skeel, R. D.; Kalé, L.; Schulten, K. Scalable Molecular Dynamics with NAMD. *J. Comput. Chem.* **2005**, *26*, 1781–1802.
- (43) Harvey, M. J.; Giupponi, G.; Fabritiis, G. De. ACEMD: Accelerating Biomolecular

- Dynamics in the Microsecond Time Scale. *J. Chem. Theory Comput.* **2009**, *5*, 1632–1639.
- (44) Wang, J.; Wolf, R. M.; Caldwell, J. W.; Kollman, P. A.; Case, D. A. Development and Testing of a General Amber Force Field. *J. Comput. Chem.* **2004**, *25*, 1157–1174.
- (45) Bayly, C. I.; Cieplak, P.; Cornell, W.; Kollman, P. A. A Well-Behaved Electrostatic Potential Based Method Using Charge Restraints for Deriving Atomic Charges: The RESP Model. *J. Phys. Chem.* **1993**, *97*, 10269–10280.
- (46) Fritschy, J.-M.; Brünig, I. Formation and Plasticity of GABAergic Synapses: Physiological Mechanisms and Pathophysiological Implications. *Pharmacol. Ther.* **2003**, *98*, 299–323.
- (47) Wang, J.; Wang, W.; Kollman, P. a; Case, D. a. Antechamber, An Accessory Software Package For Molecular Mechanical Calculations. *J. Am. Chem. Soc* **2001**, *222*, U403.
- (48) ChemAxon. ChemAxon - Software Solutions and Services for Chemistry and Biology. *MarvinSketch, Version 19.8.0*. 2019.
- (49) Barducci, A.; Bussi, G.; Parrinello, M. Well-Tempered Metadynamics: A Smoothly Converging and Tunable Free-Energy Method. *Phys. Rev. Lett.* **2008**, *100*, 020603.
- (50) Laio, A.; Parrinello, M. Escaping Free-Energy Minima. *Proc. Natl. Acad. Sci.* **2002**, *99*, 12562–12566.
- (51) Tribello, G. A.; Bonomi, M.; Branduardi, D.; Camilloni, C.; Bussi, G. PLUMED 2: New Feathers for an Old Bird. *Comput. Phys. Commun.* **2014**, *185*, 604–613.
- (52) Subramaniam, P.; Nandan, N. Effect of Xylitol, Sodium Fluoride and Triclosan

Containing Mouth Rinse on Streptococcus Mutans. *Contemp. Clin. Dent.* **2011**, 2, 287.

- (53) Datsenko, K. A.; Wanner, B. L. One-Step Inactivation of Chromosomal Genes in Escherichia Coli K-12 Using PCR Products. *Proc. Natl. Acad. Sci.* **2000**, 97, 6640–6645.

**For Table of Contents Use Only**

# **Kanamycin uptake into *Escherichia coli* is facilitated by OmpF and OmpC porin channels located in the outer membrane**

*Jayesh Arun Bafna, Eulàlia Sans-Serramitjana, Silvia Acosta-Gutiérrez, Igor Bodrenko, Daniel Hörömpöli, Anne Berscheid, Heike Brötz-Oesterhelt, Mathias Winterhalter and Matteo Ceccarelli.*

Kanamycin matches perfectly with the eyelet region and electrostatic of OmpF/OmpC. Its translocation *via* these porins is relevant for antibiotic potency, though other uptake mechanisms are not excluded

